Letter

# Critical comparison of general-purpose collective variables for crystal nucleation

Julien Lam [1,2,*] and Fabio Pietrucci [3]

[1] *CEMES, Centre National de la Recherche Scientifique and Université de Toulouse, 29 rue Jeanne Marvig, 31055 Toulouse Cedex, France*

[2] *Université Lille, Centre National de la Recherche Scientifique, INRA, ENSCL, UMR 8207, UMET, Unité Matériaux et Transformations, F 59000 Lille, France*

[3] *Sorbonne Université, Centre National de la Recherche Scientifique, UMR 7590, IMPMC, 75005 Paris, France*

(Received 25 April 2022; accepted 6 January 2023; published 24 January 2023)

The nucleation of crystals is a prominent phenomenon in science and technology that still lacks a full atomic-scale understanding. Much work has been devoted to identifying order parameters able to track the process, from the inception of early nuclei to their maturing to critical size until growth of an extended crystal. We critically assess and compare two powerful distance-based collective variables, an effective entropy derived from liquid state theory and the path variable based on permutation invariant vectors using the Kob-Andersen binary mixture and a combination of enhanced-sampling techniques. Our findings reveal a comparable ability to drive nucleation when a bias potential is applied, and comparable free-energy barriers and structural features. Yet, we also found an imperfect correlation with the committor probability on the barrier top which was bypassed by changing the order parameter definition.

DOI: 10.1103/PhysRevE.107.L012601

Numerous important phenomena in nature can be characterized as rare events, where a transition between metastable states involves the crossing of free-energy barriers [1–3]. Atomistic computer simulations of such mechanisms typically require exceedingly long trajectories so that rare spontaneous fluctuations allow for the emergence of the critical event. Tempering, biasing, and path sampling techniques have been developed to accelerate the simulations by many orders of magnitude, thus overcoming the timescale problem [4–8]. In many cases, the success of those techniques is bound to the correct definition of a collective variable (CV) able to precisely track the transition from one state to the other [9,10].

Traditionally, each CV is designed for a specific type of transition. In the case of crystallization, a paradigmatic phenomenon at the focus of large theoretical and computational efforts, the solid formation within a liquid is associated with the breaking of translational and orientational symmetries [11,12], that can be measured, e.g., via the local density [13] or the spherical harmonics analysis as proposed by Steinhardt *et al.* [14,15]. However, such order parameters are by construction related to geometrical properties of the final crystal. Using them as CVs assumes implicitly that the nucleation pathway goes through a monotonic increase of particular geometric quantities. This assumption turns out to be well adapted to simple systems including monodisperse Lennard-Jones [16] and hard spheres [17]. Yet, materials of technological interests can exhibit more complex nucleation pathways [18–21] which may not be captured by traditional CVs. Therefore, recent efforts have been dedicated to defining novel CVs that are structurally agnostic and do not constrain the nucleation pathway, constructed also by means of machine-learning techniques [22–27].

Two recent simple and physically transparent CV formulations tackle the problem of tracking order-disorder transitions based on the set of all interatomic distances: (1) the permutation invariant vector (PIV) [28], combined with the path-CV scheme [29,30], and (2) the approximate two-body entropy, combined with enthalpy [31–34]. While both CV formulations have been successful at exploring phase transitions and sampling free-energy landscapes in a range of different systems [20,33,35–39], a critical comparison between them is, to our knowledge, still lacking: this is the aim of this Letter, exploiting binary Lennard-Jones (LJ) crystallization as a nontrivial test case.

While numerous works focused on the exploration of the free-energy landscape for crystallization in mono-disperse LJ [40–43], the case of binary LJ remains only scarcely explored despite being of great interest for fundamental purposes. One of the most studied binary LJ mixtures was first introduced by Kob and Andersen more than 20 years ago [44]. In particular, the glass forming ability of this particular binary LJ fluid has been employed to tackle fundamentals of the glass transition itself [45–50]. Regarding its crystallization counterparts, more than 20 different crystal phases were found when using the Kob-Andersen (KA) interactions [51,52] and it was observed that CsCl-like crystal could rapidly be formed when the system is at the equimolar ratio [52]. To the best of our knowledge, the nucleation mechanism leading to such crystal in the equimolar ratio remains unexplored.

In this Letter, we examined the free-energy landscape of an equimolar mixture of binary KA particles by using a combination of metadynamics simulations [6,53] and umbrella sampling (US) [54,55]. We found that both CVs efficiently trigger crystallization and lead to similar free-energy barriers

*julien.lam@cnrs.fr

 

of nucleation. However, when analyzing detailed commitment probabilities [56], we show that such CVs are insufficient to discriminate with high precision the transition state. We finally demonstrate that the size of the crystal cluster provides sufficient additional information to complete the set of CVs. All simulations involve 4394 atoms with the same number of $A$ and $B$ particles interacting through a LJ model. For $AA$ interactions, we define $\epsilon$ and $\sigma$ as respectively the energy and distance LJ parameters while for the other interactions the KA model is the following [44]: $\epsilon_{AB}/\epsilon = 1.5$, $\epsilon_{BB}/\epsilon = 0.5$, $\sigma_{AB}/\sigma = 0.8$, and $\sigma_{BB}/\sigma = 0.88$. The $NPT$ ensemble is employed at $k_BT = 0.75\epsilon$ and $P = 0$ so that we have $T/T_{\text{melt}} = 0.95$ [46]. LAMMPS (version 4 Jan. 2019) [57] patched with PLUMED (version 2.5.1) [58,59] is used for the molecular dynamics (MD) simulations and OVITO [60] and PYSCAL [61] are employed for the structure analysis.

In the case of the PIV-based CV, we constructed a liquid configuration and a CsCl-type crystal which are then relaxed at the investigated thermodynamics conditions. The obtained configurations are then used as references to construct a path CV named *PIV.s* tracking the progression from liquid to crystal:

$$s = \frac{e^{-D(X,X_{\text{liq}})} + 2e^{-D(X,X_{\text{cry}})}}{e^{-D(X,X_{\text{liq}})} + e^{-D(X,X_{\text{cry}})}} \tag{1}$$

where $X$ is the atomic configuration, $\lambda = 2.3D(X_{\text{liq}}, X_{\text{cry}})$, and the metric $D$ is the squared Euclidean distance in the space of sorted vectors of distances, filtered via a rational coordination function of formula $[1-(r_{ij}/r_0)^6]/[1-(r_{ij}/r_0)^{12}]$ with $r_{ij}$ the distance between atoms and $r_0 = 1.4\sigma$. As such, the average of PIV.s is equal to 1.08 and 1.89 respectively for liquid and crystal structures.

For the second CV, we employed the effective entropy, $S$, which is approximated from liquid state theory:

$$S = -2\pi\rho k_B \int_0^\infty [g(r)\ln g(r) - g(r) + 1]r^2 dr \tag{2}$$

where $g(r)$ is the pair-distribution function computed with a cutoff at $2.5\,\sigma$ and a broadening parameter equal to $0.05\,\sigma$, $k_B$ is the Boltzmann constant, and $\rho$ is the density of the system. We note that the employed implementation of the effective entropy does not distinguish between different types of atoms. Under this formulation, the average of $S$ is equal to $-1.85$ and $-9.49$ respectively for liquid and crystal structures. More details on both methods can be found in the original papers [29,31], while PLUMED input files can be downloaded from Plumed Nest [62]. In all simulations, the system volume is constrained not to exceed more than 5% of the equilibrium liquid, to avoid sampling structures with voids. This is achieved by imposing a semiparabolic wall on the volume with an elastic constant equal to $10^3\epsilon/\sigma^3$.

In the first comparison, for each of the two CVs we performed three independent metadynamics simulations with purposely short duration thus allowing for only one barrier crossing event. The objective here was not to reach an accurate measurement of the free-energy landscape but only to rapidly find a first reactive trajectory and critical nucleus. The height of the Gaussian kernels is equal to $0.05\,\epsilon = 0.667k_BT$ in both cases. The widths are chosen as twice the standard deviation of the CVs' distribution in the liquid regime. From

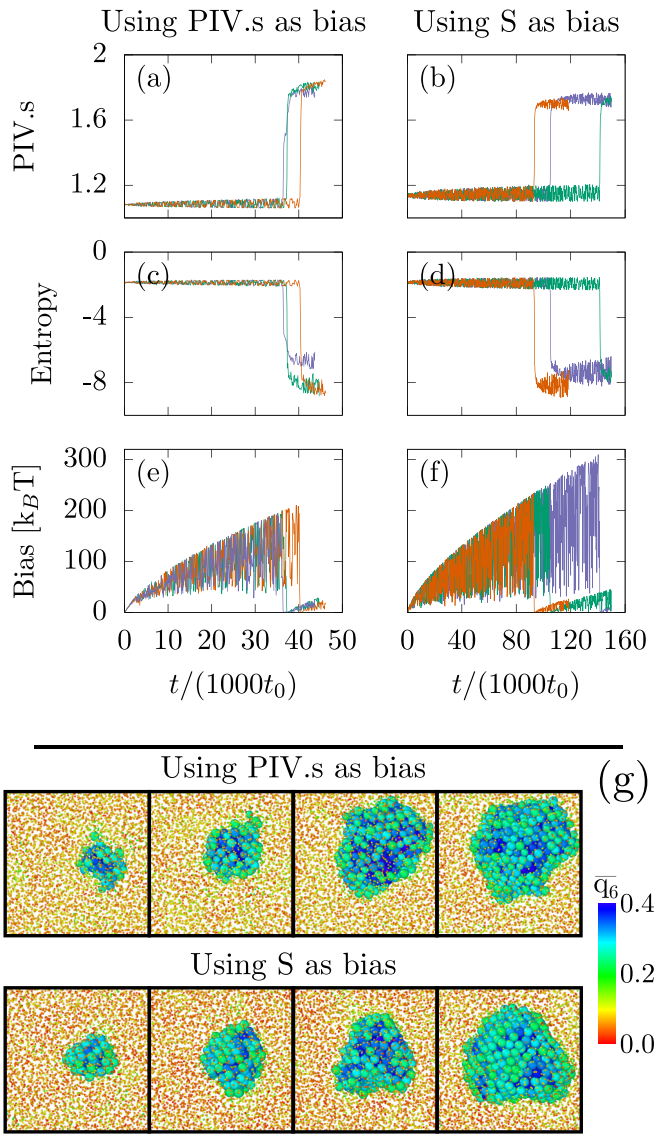


FIG. 1. (a)–(d) Temporal evolution of the collective variables during metadynamics simulations. In panels (a) and (c) and in panels (b) and (d), the biasing is made respectively using PIV-based and entropy-based collective variables. (e), (f) Corresponding temporal evolution of the metadynamics instantaneous bias that results from successive Gaussians depositions. Each color corresponds to an independent simulation. (g) Typical images of the observed nucleation event along metadynamics trajectories using the two variables. Color coding is based on the value of the averaged Steinhardt parameters [14,15] taken in their sixth order $\overline{q_6}$ and particles with $\overline{q_6}$ smaller than 0.25 are shown with a smaller size [see Supplemental Material [68] (SI.A therein) for more information].

Fig. 1, both sampling methods lead to the nucleation event with roughly the same timescales and maximum bias height. In addition, Fig. 1(g) shows that both methods do not lead to the emergence of several crystalline clusters at the same time but to a single, roughly spherical cluster following an isotropic growth. This is a remarkable result for PIV and entropy CVs: they lead to localized nucleation events despite being global order parameters. At this stage, it remains difficult to observe any difference between the two approaches.

Commitment probability analysis (CPA) consists in determining the probability to form the crystal before the liquid starting from a specific configuration, by generating a set of unbiased MD trajectories with different initial velocities drawn from the Maxwell-Boltzmann distribution [3]. We employed this technique in two stages. In the first stage, atomic configurations on the transition pathway obtained with metadynamics are used to initialize MD trajectories of relatively long duration ($>5\times10^4 t_0$). Such simulations can lead to crystal growth or melting, but can also display a cluster size lasting for a sizable time. In the second stage, we therefore use the latter configurations to identify a critical nucleus that is defined as leading to the same number of crystallization and melting trajectories from ten independent sets of velocities.

The CPA trajectories collected from this second stage are finally used to perform umbrella sampling calculations, that allow for a relatively simple control on the convergence of the free-energy landscape. By initializing with unbiased reactive trajectories, we sample a realistic crystallization pathway and we reduce the chances to observe hysteresis.

Although metadynamics simulations sample a large region of PIV.s and $S$, it remains that the nucleation barrier is located in a much more narrow phase space which will be investigated using umbrella sampling calculations. We used 50 windows with one-dimensional biases applied respectively on PIV.s and $S$. To validate the convergence of the free energy, we tested two different values of the harmonic restraint for each CV, $k = [5\times10^5; 10^6]$ and $[2\times10^4; 5\times10^4]$ for PIV.s and $S$, respectively. We applied the weighted histogram analysis method [55] comparing the last half and the last quarter of the total simulation time of each window ($4\times10^5 t_0$) in order to estimate the error bar on the free energy. We therefore obtain in Figs. 2(a) and 2(b) four free-energy curves for each CV, that appear to be similar thus showing that the free-energy calculations are well converged with a standard deviation of the barrier value respectively equal to 0.37 and 0.55 $k_BT$. At this stage, we show that the two CVs exhibit the same free-energy barrier equal to 30 $k_BT$.

After having compared both methods employing metadynamics and umbrella sampling, we confronted PIV.s and $S$ in terms of commitment probability $P_{\text{crys}}$. For that purpose, configurations obtained with umbrella sampling are used to initialize CPA. Based on results from Supplemental Material [68] (SI.B therein), we used 100 independent sets of velocities to ensure convergence of the commitment probability. Figures 2(c) and 2(d) show $P_{\text{crys}}$ as a function of the CVs. The black lines correspond to a hyperbolic tangent fit from which we extracted a critical value indicated as a dotted line in Figs. 2(a) and 2(b). In both cases, the obtained critical value only slightly differs from the maximum of the free-energy curve. Furthermore, in Figs. 2(e) and 2(f), we restricted CPA to configurations that are located near the barrier top. In both cases, it appears that instead of a peaked distribution around $P_{\text{crys}} = 0.5$, an indication of an optimal reaction coordinate [3], we obtain distributions that have significant values in the whole range from zero to one. This demonstrates that both PIV.s and $S$ are suboptimal CVs that cannot precisely discriminate transition states from structures committed to the crystal or to the liquid.

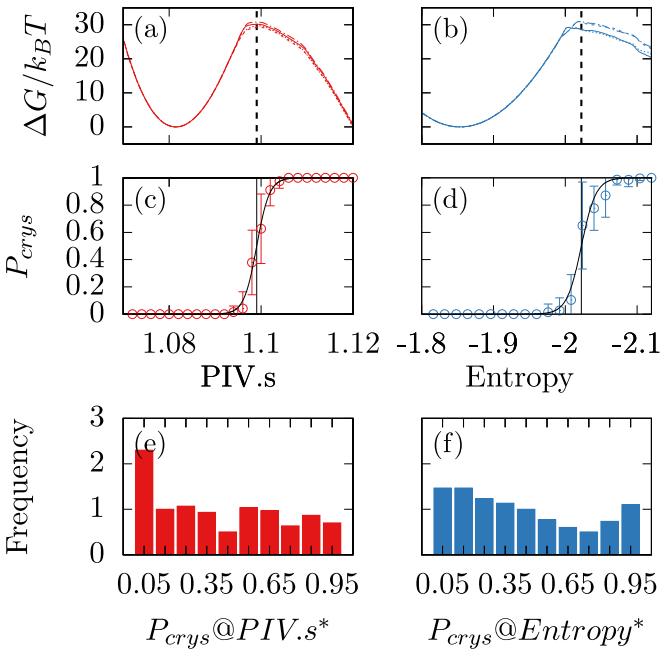


FIG. 2. (a), (b) Free-energy barriers obtained with umbrella sampling using (a) PIV.s and (b) $S$ as CV. The dotted lines indicate the transition-state CV values as obtained from CPA. (c), (d) Commitment probability for the two CVs (c) PIV.s and (d) $S$: the dotted lines indicate the critical value deduced from a fit of the data set. (e), (f) Commitment distribution extracted from all of the obtained transition-state configurations with (e) PIV.s (300 samples) and (f) $S$ (300 samples).

We further investigated the issue of the quantitative comparison of free-energy barriers estimated from different CVs. In Supplemental Material [68] (SI.C therein) we report calculations using a second definition of PIV.s based on a shorter-range switching function (i.e., including poorer information about atomic environments compared to the original one). The free-energy barrier estimated from US with the latter lower-quality CV differs by a significant amount (7 $k_BT$ representing 25%) compared to what was obtained with both the original PIV.s and $S$, with the commitment distribution still exhibiting a suboptimal behavior. This result points to the relevance of developing algorithms combining CV optimization and sampling acceleration in order to obtain accurate barriers [25,26,63].

To shed light on the issue related to the nonpeaked distribution of CPA, we inspected the size of the largest crystalline cluster, $N_{\text{crys}}$, by computing the value of Steinhardt's bond-orientational order parameter averaged over the first neighbor shell, and defined ordered atoms as having $q_6$ larger than 0.25 [14,15]. In order to identify the shortcomings in the employed CVs, we focused on structures that were selected in Figs. 2(e) and 2(f) and plot their commitment probability $P_{\text{crys}}$ as a function of $N_{\text{crys}}$ [see Figs. 3(a) and 3(b)]. When filtered at critical values of PIV.s or $S$, $P_{\text{crys}}$ again exhibits a clear correlation with $N_{\text{crys}}$, indicating that the combination of $N_{\text{crys}}$ along with PIV.s or $S$ might constitute an improved CV for the crystallization pathway. Finally, we computed the critical values of $N_{\text{crys}}$ using the hyperbolic tangent fit, obtaining 316

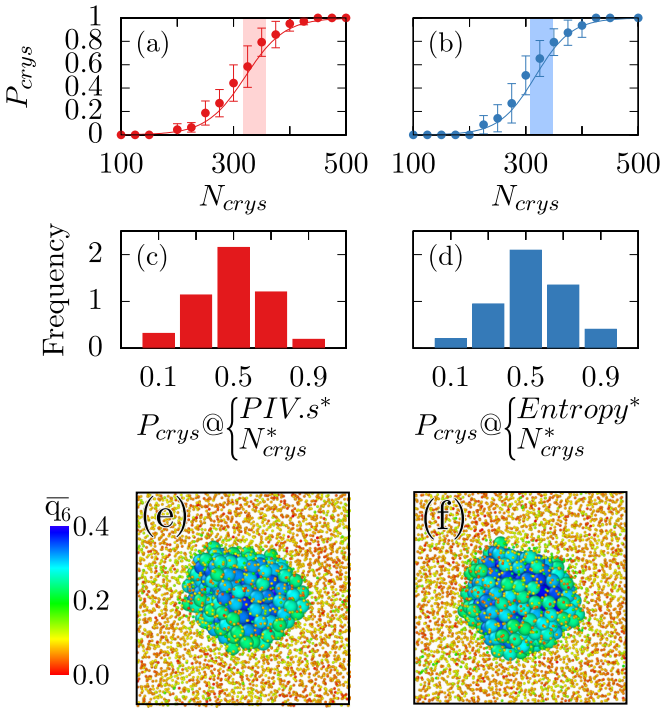


FIG. 3. (a), (b) Commitment probability as a function of $N_{\text{crys}}$ at fixed critical values of (c) PIV.s and (d) $S$. The black lines indicate a hyperbolic tangent fit of the whole data set. (c), (d) Commitment probability distribution obtained with (c) PIV.s and (d) $S$ when also constraining the value of $N_{\text{crys}} \in [305{:}345]$. (e), (f) Typical aspect of the critical nucleation cluster, defined as having $P_{\text{crys}} = 0.5$. Color coding is based on the value of $\overline{q_6}$ and particles with $\overline{q_6}$ smaller than 0.25 are shown with a smaller size.

and 321 atoms respectively for the $S$-based and PIV.s-based datasets. As shown in Figs. 2(c) and 2(d), the $P_{\text{crys}}$ distributions corresponding to the critical values of simultaneously $N_{\text{crys}}$ and either PIV.s or $S$, albeit obtained with fewer points than in Figs. 2(e) and 2(f) (74 for $S$ and 79 for PIV.s), are clearly peaked around 0.5 in both cases. This latter result confirms that both PIV.s and $S$ are improved in their ability to resolve transition state structures by combining them with $N_{\text{crys}}$.

We note that based on these results it can be natural to ask if $N_{\text{crys}}$ alone provides a good committor distribution. Results shown in Supplemental Material [68] (SI. D therein) demonstrate that when taken alone $N_{\text{crys}}$ is similar to both $S$ and PIV. Indeed, although $N_{\text{crys}}$ positively correlates with the committor probability, the distribution at the critical value of $N_{\text{crys}}$ does not lead to a narrow-peaked distribution centered around 0.5. Further analysis of potential correlations between $N_{\text{crys}}$ and the investigated CVs can be found in Supplemental Material [68] (SI.E therein). As such, we confirm the need to combine $S$ or PIV.s with $N_{\text{crys}}$. Finally, this Letter comparing the use of PIV and $S$ as order parameters gives also insights into the crystallization mechanisms in the Kob-Andersen equimolar binary Lennard-Jones system. Indeed, all of the configurations with a commitment probability between 0.4 and 0.6 are collected and characterized in terms of atomic structure [see Table I and Figs. 3(e) and 3(f)]. First, results

TABLE I. Structural properties of the critical cluster as obtained with PIV.s and $S$.

| | PIV.s | Entropy |
|---|---|---|
| $\overline{q_6}$ | $0.35 \pm 0.01$ | $0.36 \pm 0.01$ |
| $\overline{q_4}$ | $0.041 \pm 0.001$ | $0.041 \pm 0.001$ |
| $N_{\text{crys}}$ | $340 \pm 33$ | $336 \pm 32$ |
| Radius [$\sigma$] | $3.03 \pm 0.11$ | $2.99 \pm 0.09$ |
| Asphericity | $0.22 \pm 0.07$ | $0.21 \pm 0.07$ |
| Composition | $0.482 \pm 0.091$ | $0.479 \pm 0.092$ |
| $N^A_{\text{SC}}/N^B_{\text{SC}}$ | $1.08 \pm 0.04$ | $1.07 \pm 0.04$ |
| $(N^A_{\text{SC}} + N^B_{\text{SC}})/N_{\text{crys}}$ | $0.98 \pm 0.12$ | $0.99 \pm 0.13$ |

obtained with both methods seem to lead to similar results. In particular, the size of the nucleus is around 335 atoms which correspond to radii around 3 Å. We note that although the critical nucleus is not extending through the periodic boundary conditions our results may still suffer from finite size since we have 4394 particles and 340 in the critical nucleus. Regarding the binary ratio, the critical nucleus almost respects that of the equimolar mixture which suggests that chemical ordering is directly reached during the nucleation event. The small value of the asphericity demonstrates that the nucleus is mostly spherical [see Figs. 3(e) and 3(f)]. One final structural measurement for the obtained critical clusters concerns the chemical ordering since the Kob-Andersen mixture is supposed to crystallize with the CsCl chemical ordering. For that purpose, we measured $N^A_{\text{SC}}$ (resp. $N^B_{\text{SC}}$), the number of single cubic atoms when isolating atoms of type $A$ (resp. $B$), using the Polyhedral template matching algorithm as implemented in OVITO. Results in Table I show that there is almost the same number of $A$ and $B$ single cubic atoms and that most of the crystalline structures within the critical cluster are made of $A$ and $B$ single cubic atoms, thus confirming that the obtained critical clusters follow the CsCl chemical ordering.

A large body of literature indicates that crystal nucleation is a complex process, with several features that are system independent (captured to some extent by classical nucleation theory) and others that are specific to the materials and conditions. Our results carry new insight into this old problem and allow us to draw several conclusions.

First, the two CVs under examination (the PIV-based path coordinate and the entropy-based coordinate), albeit different in formulation, have a comparable performance on the binary Kob-Andersen system. In particular, both CVs lead to statistically converging free-energy landscapes via umbrella sampling. Yet, because the commitment distribution is not centered around 0.5 at the critical barrier, the obtained value for the barrier is likely misestimated when compared to a more optimal reaction coordinate, so that an accurate nucleation rate cannot be deduced. Meanwhile, they allow one to accelerate via metadynamics the formation and growth of crystal nuclei from the liquid. This result is nontrivial to achieve in generic systems, as testified by the difficult cases of ice (tackled with the PIV-based coordinates in Ref. [29], and combining the entropy-based coordinate with an *ad hoc* structural fingerprint in Ref. [64]) and $CO_2$, and methane hydrates nucleation [65,66].

Detailed inspection of the kinetic fate of atomic configurations found at the barrier top (the committor probability histogram) indicates however that the two coordinates are suboptimal, and can be improved by including additional degrees of freedom such as those encoded in Steinhardt-based nucleus-size indicators. This result is, again, nontrivial since the latter class of order parameters, although well adapted in the simple case of the single-component Lennard-Jones system [41–43,67], can be suboptimal for systems undergoing a complex nonclassical nucleation pathway traversing polymorphic and/or disordered structures.

The results of this Letter represent a manifestation of the well-known "chicken and egg" paradox in the field of rare-events sampling and free-energy calculations: optimal CVs are necessary to accelerate the sampling of a transition in order to explore the most relevant mechanisms, while, at the same time, a detailed knowledge of the most relevant mechanisms is necessary to design beforehand optimal CVs.

A broad consensus identifies the optimal CV for a transition between two metastable states with the committor function: unfortunately, information about committor values can be obtained in practical cases only in a very small subset of configuration space, for instance in the vicinity of a barrier top explored with metadynamics, transition path sampling, or other techniques. A CV optimized to represent the committor in such a small configurational subset [10], when used in combination with biased sampling techniques like metadynamics or umbrella sampling, is likely to drive the system towards suboptimal transition mechanisms and hysteresis effects, because such a CV ignores the behavior of the committor in the entirety of configurational space.

For the same reason, computing the committor histogram for CVs in a small subset of configurational space, as done in this Letter and, customarily, in many recent works, is a useful test that, unfortunately, even when passed offers no guarantees about the optimality of the same CVs in other regions of configuration space. Only estimating the committor for all possible configurations, an impossible task, would yield an optimal CV that guarantees optimal biased dynamics. This is the main reason why biased dynamics, albeit powerful, always needs to be used and interpreted with care.

Considering the many challenges posed by the investigation of rare events, we propose the approach in the present Letter as a good compromise to bridge the communities exploiting transition path sampling and CV-biasing techniques, providing at the same time important information in the context of the development of machine-learning CV optimization algorithms.

Research funded by Fonds De La Recherche Scientifique–FNRS (32729323). Computational resources have been provided by the Consortium des Equipements de Calcul Intensif and by the Fédération Lyonnaise de Modélisation et Sciences Numériques. J.L. thanks James F. Lutsko and Pablo P. Piaggi for fruitful discussions. J.L. is also grateful to Sarath Menon for his help in the use of PYSCAL and Daniel Forster for helping with the computation of asphericity.

[1] S. K. Jha and J. B. Udgaonkar, Curr. Sci. **99**, 457 (2010).
[2] G. C. Sosso, J. Chen, S. J. Cox, M. Fitzner, P. Pedevilla, A. Zen, and A. Michaelides, Chem. Rev. **116**, 7078 (2016).
[3] S. Jungblut and C. Dellago, Eur. Phys. J. E **39**, 77 (2016).
[4] O. Valsson, P. Tiwary, and M. Parrinello, Annu. Rev. Phys. Chem. **67**, 159 (2016).
[5] F. Pietrucci, Rev. Phys. **2**, 32 (2017).
[6] G. Bussi and A. Laio, Nat. Rev. Phys. **2**, 200 (2020).
[7] P. G. Bolhuis, D. Chandler, C. Dellago, and P. L. Geissler, Annu. Rev. Phys. Chem. **53**, 291 (2002).
[8] F. A. Escobedo, E. E. Borrero, and J. C. Araque, J. Phys.: Condens. Matter **21**, 333101 (2009).
[9] D. Wales, *Energy Landscapes Applications to Clusters, Biomolecules and Glasses*, Cambridge Core (Cambridge University Press, Cambridge, England, UK, 2004).
[10] B. Peters, Annu. Rev. Phys. Chem. **67**, 669 (2016).
[11] J. Russo and H. Tanaka, Sci. Rep. **2**, 505 (2012).
[12] Y.-W. Li and Z.-Y. Sun, Soft Matter **12**, 2009 (2016).
[13] J. F. Lutsko and G. Nicolis, Phys. Rev. Lett. **96**, 046102 (2006).
[14] P. J. Steinhardt, D. R. Nelson, and M. Ronchetti, Phys. Rev. B **28**, 784 (1983).
[15] W. Lechner and C. Dellago, J. Chem. Phys. **129**, 114707 (2008).
[16] F. Trudu, D. Donadio, and M. Parrinello, Phys. Rev. Lett. **97**, 105701 (2006).
[17] S. Auer and D. Frenkel, Nature (London) **409**, 1020 (2001).
[18] C. Desgranges and J. Delhommelle, Phys. Rev. Lett. **123**, 195701 (2019).
[19] S. Bechelli, B. Gonzalez, V. Piquet, I. Essafri, C. Desgranges, and J. Delhommelle, J. Phys. Chem. B **121**, 8558 (2017).
[20] J. Amodeo, F. Pietrucci, and J. Lam, J. Phys. Chem. Lett. **11**, 8060 (2020).
[21] Y. Liang, G. Díaz Leines, R. Drautz, and J. Rogal, J. Chem. Phys. **152**, 224504 (2020).
[22] L. Bonati, V. Rizzi, and M. Parrinello, J. Phys. Chem. Lett. **11**, 2998 (2020).
[23] M. M. Sultan and V. S. Pande, J. Chem. Phys. **149**, 094106 (2018).
[24] A. Ma and A. R. Dinner, J. Phys. Chem. B **109**, 6769 (2005).
[25] J. M. L. Ribeiro, P. Bravo, Y. Wang, and P. Tiwary, J. Chem. Phys. **149**, 072301 (2018).
[26] W. Chen and A. L. Ferguson, J. Comput. Chem. **39**, 2079 (2018).
[27] J. Rogal, E. Schneider, and M. E. Tuckerman, Phys. Rev. Lett. **123**, 245701 (2019).
[28] G. A. Gallet and F. Pietrucci, J. Chem. Phys. **139**, 074101 (2013).
[29] S. Pipolo, M. Salanne, G. Ferlat, S. Klotz, A. M. Saitta, and F. Pietrucci, Phys. Rev. Lett. **119**, 245701 (2017).
[30] D. Branduardi, F. L. Gervasio, and M. Parrinello, J. Chem. Phys. **126**, 054103 (2007).
[31] P. M. Piaggi, O. Valsson, and M. Parrinello, Phys. Rev. Lett. **119**, 015701 (2017).

[32] P. M. Piaggi and M. Parrinello, J. Chem. Phys. **147**, 114112 (2017).
[33] P. M. Piaggi and M. Parrinello, Proc. Natl. Acad. Sci. USA **115**, 10251 (2018).
[34] M. H. Nafar Sefiddashti, B. J. Edwards, and B. Khomami, Macromolecules **53**, 10487 (2020).
[35] F. Pietrucci and R. Martoňák, J. Chem. Phys. **142**, 104704 (2015).
[36] M. Fitzner, G. C. Sosso, F. Pietrucci, S. Pipolo, and A. Michaelides, Nat. Commun. **8**, 2257 (2017).
[37] L. E. Bove, F. Pietrucci, A. M. Saitta, S. Klotz, and J. Teixeira, J. Chem. Phys. **151**, 044503 (2019).
[38] S. Schaack, Ph. Depondt, M. Moog, F. Pietrucci, and F. Finocchi, J. Chem. Phys. **152**, 024504 (2020).
[39] D. Mendels, J. McCarty, P. M. Piaggi, and M. Parrinello, J. Phys. Chem. C **122**, 1786 (2018).
[40] M. A. van der Hoef, J. Chem. Phys. **113**, 8142 (2000).
[41] P. R. ten Wolde, M. J. Ruiz-Montero, and D. Frenkel, J. Chem. Phys. **104**, 9932 (1996).
[42] P. R. ten Wolde, M. J. Ruiz-Montero, and D. Frenkel, Phys. Rev. Lett. **75**, 2714 (1995).
[43] D. Moroni, P. R. ten Wolde, and P. G. Bolhuis, Phys. Rev. Lett. **94**, 235703 (2005).
[44] W. Kob and H. C. Andersen, Phys. Rev. E **51**, 4626 (1995).
[45] T. S. Ingebrigtsen, J. C. Dyre, T. B. Schrøder, and C. P. Royall, Phys. Rev. X **9**, 031016 (2019).
[46] U. R. Pedersen, T. B. Schrøder, and J. C. Dyre, Phys. Rev. Lett. **120**, 165501 (2018).
[47] P. Crowther, F. Turci, and C. P. Royall, J. Chem. Phys. **143**, 044503 (2015).
[48] F. Turci, C. P. Royall, and T. Speck, Phys. Rev. X **7**, 031028 (2017).
[49] A. Banerjee, S. Chakrabarty, and S. M. Bhattacharyya, J. Chem. Phys. **139**, 104501 (2013).
[50] U. K. Nandi, A. Banerjee, S. Chakrabarty, and S. M. Bhattacharyya, J. Chem. Phys. **145**, 034503 (2016).
[51] T. F. Middleton, J. Hernández-Rojas, P. N. Mortenson, and D. J. Wales, Phys. Rev. B **64**, 184201 (2001).
[52] J. R. Fernández and P. Harrowell, Phys. Rev. E **67**, 011403 (2003).
[53] A. Laio and M. Parrinello, Proc. Natl. Acad. Sci. USA **99**, 12562 (2002).
[54] G. M. Torrie and J. P. Valleau, J. Comput. Phys. **23**, 187 (1977).
[55] B. Roux, Comput. Phys. Commun. **91**, 275 (1995).
[56] P. G. Bolhuis, C. Dellago, and D. Chandler, Faraday Discuss. **110**, 421 (1998).
[57] S. Plimpton, J. Comput. Phys. **117**, 1 (1995).
[58] G. A. Tribello, M. Bonomi, D. Branduardi, C. Camilloni, and G. Bussi, Comput. Phys. Commun. **185**, 604 (2014).
[59] M. Bonomi, G. Bussi, C. Camilloni, G. A. Tribello, P. Banáš, A. Barducci, M. Bernetti, P. G. Bolhuis, S. Bottaro, D. Branduardi, R. Capelli, P. Carloni, M. Ceriotti, A. Cesari, H. Chen, W. Chen, F. Colizzi, S. De, M. De La Pierre, D. Donadio, V. Drobot, B. Ensing, A. L. Ferguson, M. Filizola, J. S. Fraser, H. Fu, P. Gasparotto, F. L. Gervasio, F. Giberti, A. Gil-Ley, T. Giorgino, G. T. Heller, G. M. Hocky, M. Iannuzzi, M. Invernizzi, K. E. Jelfs, A. Jussupow, E. Kirilin, A. Laio, V. Limongelli, K. Lindorff-Larsen, T. Löhr, F. Marinelli, L. Martin-Samos, M. Masetti, R. Meyer, A. Michaelides, C. Molteni, T. Morishita, M. Nava, C. Paissoni, E. Papaleo, M. Parrinello, J. Pfaendtner, P. Piaggi, G. Piccini, A. Pietropaolo, F. Pietrucci, S. Pipolo, D. Provasi, D. Quigley, P. Raiteri, S. Raniolo, J. Rydzewski, M. Salvalaglio, G. C. Sosso, V. Spiwok, J. Šponer, D. W. H. Swenson, P. Tiwary, O. Valsson, M. Vendruscolo, G. A. Voth, A. White, and The PLUMED consortium, Nat. Methods **16**, 670 (2019).
[60] A. Stukowski, Modelling Simul. Mater. Sci. Eng. **18**, 015012 (2009).
[61] S. Menon, G. D. Leines, and J. Rogal, J. Open Source Softw. **4**, 1824 (2019).
[62] Plumed Nest, plumID23.002.
[63] M. Badaoui, P. J. Buigues, D. Berta, G. M. Mandana, H. Gu, T. Foldes, C. J. Dickson, V. Hornak, M. Kato, C. Molteni *et al.*, J. Chem. Theory Comput. **18**, 2543 (2022).
[64] H. Niu, Y. I. Yang, and M. Parrinello, Phys. Rev. Lett. **122**, 245501 (2019).
[65] A. Null, A. Berendsen Thom, and G. Bolhuis Peter, Proc. Natl. Acad. Sci. USA **116**, 19305 (2019).
[66] A. Arjun and P. G. Bolhuis, J. Chem. Phys. **154**, 164507 (2021).
[67] H. Wang, H. Gould, and W. Klein, Phys. Rev. E **76**, 031604 (2007).
[68] See Supplemental Material at http://link.aps.org/supplemental/10.1103/PhysRevE.107.L012601 for crystal structure analysis, convergence analysis of CPA, alternative expression of the PIV-based CV, CPA analysis for $N_{\mathrm{crys}}$ alone and correlation between $N_{\mathrm{crys}}$ and the other CVs.